

# Magnetoresistance oscillations induced by geometry in a two-dimensional quantum ring

Francisco A. G. de Lira,<sup>1,2,\*</sup> Edilberto O. Silva,<sup>1,†</sup> and Christian D. Santangelo<sup>2,‡</sup>

<sup>1</sup>*Departamento de Física, Universidade Federal do Maranhão, 65085-580, São Luís, Maranhão, Brazil*

<sup>2</sup>*Physics Department, Syracuse University, 13244 Syracuse, New York, United States*

(Dated: June 24, 2024)

In this work, we investigate the effects of a controlled conical geometry on the electric charge transport through a two-dimensional quantum ring weakly coupled to both the emitter and the collector. These mesoscopic systems are known for being able to confine highly mobile electrons in a defined region of matter. Particularly, we consider a GaAs device having an average radius of 800 nm in different regimes of subband occupation at non-zero temperature and under the influence of a weak and uniform background magnetic field. Using the adapted Landauer formula for the resonant tunneling and the energy eigenvalues, we explore how the modified surface affects the Van-Hoove conductance singularities and the magnetoresistance interference patterns resulting from the Aharonov-Bohm oscillations of different frequencies. Magnetoresistance oscillations depending only on the curvature intensity are reported, providing a new feature that represents an alternative way to optimize the transport through the device by tuning its geometry.

## I. INTRODUCTION

The surge of interest in studying physical phenomena arising from quantum loop systems emerged due to the noted effect proposed by Y. Aharonov and D. Bohm in 1959 [1]. Later, upon the development of the first Metal-Oxide Semiconductor Field Transistor (MOSFET) in 1960 [2], the prediction of integer quantum Hall effect quantization in 1975 [3] and its first observation in 1980 [4], R. B. Laughlin proposed a thought experiment using a metallic loop in 1981 to show that quantized Hall conductivity is a consequence of gauge invariance [5]. In the early '90s, M. Büttiker, Y. Imry, and R. Landauer predicted the existence of persistent current in non-superconducting metal loops [6, 7], which was experimentally observed years later [8, 9]. Furthermore, in 1993, Maily et al. successfully performed these experiments in semiconductor rings [10].

In recent years, experiments [11–13] and theoretical models [14, 15] have explored and predicted important aspects of these systems in more detail, including their electronic, magnetic, thermodynamic, transport, optical, and quantum informational properties [16–20]. These studies have been leading the development of several applications in technology, such as THz detectors [21], improved solar cell efficiency [22], memory devices [19], single-photon emitters [23, 24] and qubits for quantum computing [25, 26].

Although this field is very diverse, a considerable branch of these investigations has recently turned to understand how geometry affects the properties of quantum rings and other structures able to confine electrons [27–33] due to the existence of a purely geometrical potential

arising from curvature as a result of the procedure implemented by R. T. C. da Costa [34]. This is, indeed, an important concern due to the presence of topological defects in solid and liquid crystals, such as disclinations and screw dislocations [35–37]. Also, materials engineering has already made it possible to develop two-dimensional lattices with different geometries by modifying part of the structure [38, 39].

Against this backdrop, conductance plays a key role since it is a quantity of great experimental interest [40–42]. Thus, in this work, we investigate the effects of a disclination, described by the geometry of a cone, on the electric charge transport properties. In particular, we consider a two-dimensional quantum ring of GaAs with an average radius of 800 nm at the temperature of 40 mK and under the influence of a weak background magnetic field. We explore two regimes of fixed electron occupation: one (0.5 meV) and four occupied subbands (2 meV) [43].

This paper is outlined as follows. In Sec. II, we describe the model and the main aspects of differential geometry to introduce the concept of geometric potential. In Sec. III, the basic concepts of charge transport, such as quantum of conductance, resonant tunneling, and coherent and incoherent transmission, are presented. In Sec. IV, we show and discuss the effect of the modified surface in the conductance in terms of the Fermi energy, the behavior of the total and average magnetoresistance with the magnetic field for different regimes of curved surface, highlighting an interesting and almost periodic dependence with the curvature parameter. Finally, we summarize the results in Sec. V.

## II. TWO-DIMENSIONAL QUANTUM RING WITH CONICAL GEOMETRY

The system of interest is a two-dimensional quantum ring weakly coupled to two leads working as a source and

\* [goncalves.francisco@discente.ufma.br](mailto:goncalves.francisco@discente.ufma.br)  
[francisco.augoncalves@gmail.com](mailto:francisco.augoncalves@gmail.com)

† [edilberto.silva@ufma.br](mailto:edilberto.silva@ufma.br)

‡ [cgsantan@syr.edu](mailto:cdsantan@syr.edu)

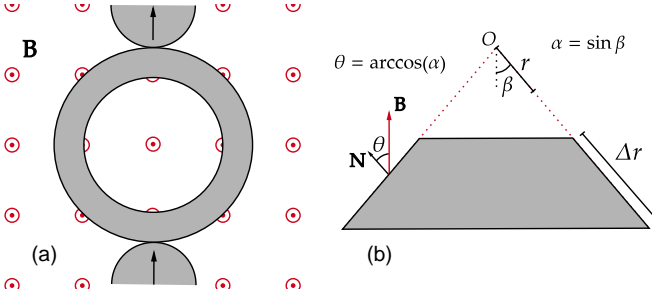


FIG. 1: (a) (Color online) Schematic illustration in an upper view of the weakly coupled ring model used in this work, adapted from [43]. (b) A side view of the model highlights the conical geometry of the ring surface for  $\alpha < 1$ . The origin is set on the virtual apex of the conical surface defined by the ring.

a drain, also called emitter and collector. The device is located in a region with a weak background magnetic field, as illustrated in Fig. 1a. The problem can be described using the theoretical model proposed by W. Tan and J. Inkson [14], which provides a radial confining potential for the two-dimensional electron gas (2DEG) depending on two parameters,  $a_1$  and  $a_2$ , in the form

$$V(r) = \frac{a_1}{r^2} + a_2 r^2 - 2\sqrt{a_1 a_2}. \quad (1)$$

These parameters can be measured experimentally and be suitably controlled to describe other similar systems, such as the quantum dot ( $a_1 = 0$ ) and the antidot ( $a_2 = 0$ ). This potential has a minimum at  $r_0 = (a_1/a_2)^{1/4}$ , the average radius of the ring. Near this point, we can approximate expression (1) as a parabola,  $V(r) \approx \mu\omega_0^2(r - r_0)^2/2$ , from which we can define  $\omega_0 = \sqrt{8a_2/\mu}$  as a frequency related to the strength of the confinement where  $\mu$  is the electron effective mass. Moreover, if the system has a total Fermi energy  $E_F$ , we can define an effective width,

$$\Delta r = \sqrt{\frac{8E_F}{\mu\omega_0^2}}. \quad (2)$$

We are interested in investigating the effects of curvature in the surface defined by this two-dimensional quantum ring. More precisely, we are concerned with the conical geometry described by the parametric equation (See Fig.1b)

$$\mathbf{x}(r, \theta) = (\alpha r \cos \theta, \alpha r \sin \theta, -r\sqrt{1 - \alpha^2}), \quad (3)$$

where  $r \in \mathbb{R}^+$  and  $0 \leq \theta \leq 2\pi$  are the surface parameters and  $0 < \alpha \leq 1$  is the curvature parameter. The line element is obtained from the coefficients of the first fundamental form  $E = \mathbf{x}_{rr} \cdot \mathbf{x}_{rr} = 1$ ,  $F = \mathbf{x}_{r\varphi} \cdot \mathbf{x}_{r\varphi} = 0$  and  $G = \mathbf{x}_{\varphi\varphi} \cdot \mathbf{x}_{\varphi\varphi} = \alpha^2 r^2$ , as

$$ds^2 = g_{ij}x^i x^j = dr^2 + \alpha^2 r^2 d\varphi^2. \quad (4)$$

If we consider a magnetic field in  $z$  direction, the unit normal vector of the surface

$$\mathbf{N} = (\sqrt{1 - \alpha^2} \cos \varphi, \sqrt{1 - \alpha^2} \sin \varphi, \alpha) \quad (5)$$

is no longer parallel to  $\mathbf{B}$  if  $\alpha \neq 1$ . Thus, the corresponding vector potential will be [44]

$$\mathbf{A} = \frac{B}{2} \hat{e}_\varphi = \frac{B}{2} \alpha r \hat{\varphi}. \quad (6)$$

Note that the curl of the vector potential (6), for which  $\mathbf{N}$  is the orthonormal basis vector instead of  $\hat{z}$ , is equal to  $B\alpha\mathbf{N}$ . This is just the component of  $B$  in the normal direction since  $\alpha = \cos \theta$  (Fig. 1b).

The R. T. C da Costa procedure [34] of confining a quantum particle to a surface tells us that this particle experiences a purely geometric potential arising from the curvature of the surface. With the coefficients of the second fundamental form  $e = \mathbf{x}_{rr} \cdot \mathbf{N} = 0$ ,  $f = \mathbf{x}_{r\varphi} \cdot \mathbf{N} = 0$  and  $g = \mathbf{x}_{\varphi\varphi} \cdot \mathbf{N} = -\alpha r \sqrt{1 - \alpha^2}$ , we can explicitly find an expression for the geometric potential

$$V_S = -\frac{\hbar^2}{2\mu} (M^2 - K), \quad (7)$$

where

$$M = \frac{Eg - 2Ff + Ge}{2(EG - F^2)} \quad \text{and} \quad K = \frac{eg - f^2}{EG - F^2} \quad (8)$$

are the mean and Gaussian curvatures, respectively. Thus, the geometric potential for the parametric surface in (3) is given by the expression [45]

$$V_S = -\frac{\hbar^2}{2\mu} \left[ \frac{(1 - \alpha^2)}{4\alpha^2 r^2} - \left( \frac{1 - \alpha}{\alpha} \right) \frac{\delta(r)}{r} \right]. \quad (9)$$

We can clearly see that this potential provides an attractive force towards the center of the ring (conic apex), whereas an extremely repulsive contribution exists at its very center.

The corresponding two-dimensional Schrödinger equation of the system can now be computed in its general form as

$$\begin{aligned} E\chi_S = & -\frac{\hbar^2}{2m_t} \left[ \frac{1}{\sqrt{g}} \frac{\partial}{\partial q^i} \left( \sqrt{g} g^{ij} \frac{\partial \chi_S}{\partial q^j} \right) \right] \\ & -\frac{\hbar^2}{2m_t} \left[ \frac{ie}{\hbar \sqrt{g}} \frac{\partial}{\partial q^i} (\sqrt{g} g^{ij} A_j) \chi_S \right] \\ & -\frac{\hbar^2}{2m_t} \left[ \frac{2ie}{\hbar} g^{ij} A_i \frac{\partial \chi_S}{\partial q^j} - \frac{e^2}{\hbar^2} g^{ij} A_i A_j \chi_S \right] \\ & -V_S \chi_S + \left( \frac{a_1}{r^2} + a_2 r^2 - V_0 \right) \chi_S, \end{aligned} \quad (10)$$

where  $\chi_S = \chi_S(r, \varphi)$  represents the surface wavefunction resulting from the da Costa procedure [34] and  $i, j = \{1, 2\}$ . Using result (4) and (9) in the last expression, we

obtain the explicit equation for the conical geometry

$$\begin{aligned}
& -\frac{\hbar^2}{2\mu} \left[ \frac{1}{r} \frac{\partial}{\partial r} \left( r \frac{\partial}{\partial r} \right) - \frac{e^2 B^2 \alpha^2 r^2}{4\hbar^2} + \frac{1}{\alpha^2 r^2} \left( \frac{\partial}{\partial \varphi} + i l \right)^2 \right] \chi_S \\
& - \frac{\hbar^2}{2\mu} \frac{ieB}{\hbar} \left( \frac{\partial}{\partial \varphi} + i l \right) - \frac{\hbar^2}{2\mu} \left[ \frac{(1-\alpha^2)}{4\alpha^2 r^2} - \left( \frac{1-\alpha}{\alpha} \right) \frac{\delta(r)}{r} \right] \chi_S \\
& + \left( \frac{a_1}{r^2} + a_2 r^2 - V_0 \right) \chi_S = E \chi_S. \tag{11}
\end{aligned}$$

Proposing solutions of the form  $\chi_S(r, \varphi) = e^{im\varphi} f(r)$  in the previous expression, we obtain the radial differential equation

$$\begin{aligned}
& \frac{d^2 f}{dr^2} + \frac{1}{r} \frac{df}{dr} - \left[ \frac{2\mu a_2}{\hbar^2} + \frac{e^2 B^2 \alpha^2}{4\hbar^2} \right] r^2 f(r) \\
& - \frac{1}{r^2} \left[ \frac{2\mu a_1}{\hbar^2} + \frac{(m-l)^2}{\alpha^2} - \frac{(1-\alpha^2)}{4\alpha^2} \right] f(r) \\
& - \left\{ \left[ \frac{eB(m-l)}{\hbar} + \frac{2\mu(E+V_0)}{\hbar^2} \right] - \frac{(1-\alpha)}{\alpha r} \delta(r) \right\} f(r) = 0, \tag{12}
\end{aligned}$$

from which is useful to define

$$\frac{2\mu a_2}{\hbar^2} + \frac{e^2 B^2 \alpha^2}{4\hbar^2} = \frac{1}{4\lambda^4} \quad \text{and} \quad \omega = \sqrt{\omega_0^2 + (\alpha\omega_c)^2}, \tag{13}$$

as the effective magnetic length  $\lambda = \sqrt{\hbar/\mu\omega}$  and  $\omega_c = eB/\mu$  as the cyclotron frequency. Moreover, we can rewrite

$$L = \sqrt{\frac{2\mu a_1}{\hbar^2} + \frac{(m-l)^2}{\alpha^2} - \frac{(1-\alpha^2)}{4\alpha^2}} \tag{14}$$

and

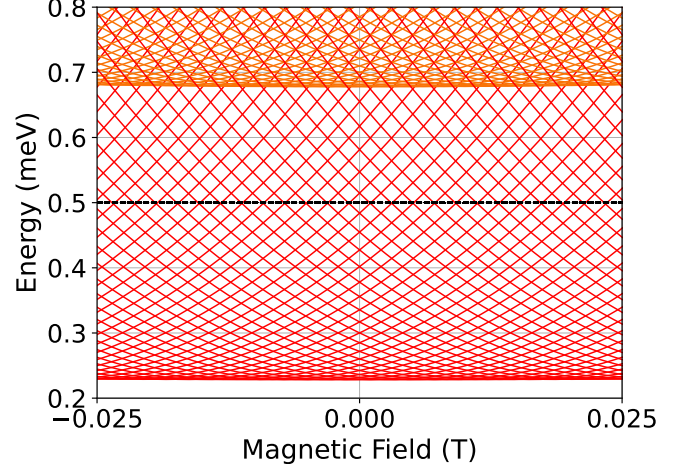
$$S = \sqrt{\frac{eB(m-l)}{\hbar} + \frac{2\mu(E+V_0)}{\hbar^2}}, \tag{15}$$

in order to remain with a compact form for the radial differential equation (12) [32]

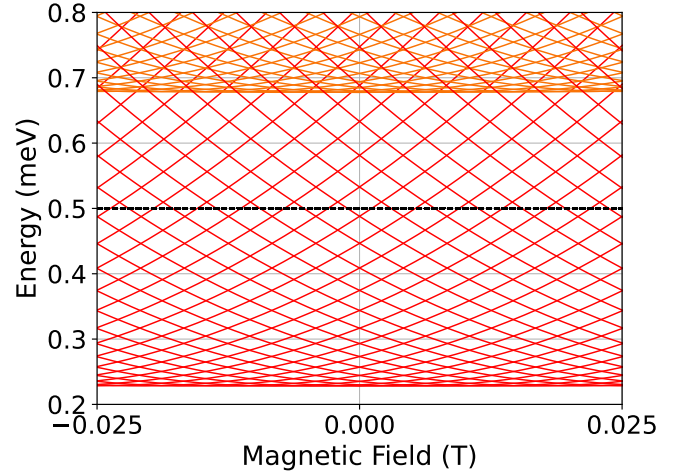
$$\frac{d^2 f}{dr^2} + \frac{1}{r} \frac{df}{dr} - \left[ \frac{r^2}{4\lambda^4} + \frac{L^2}{r^2} - S^2 + \frac{(1-\alpha)}{\alpha r} \delta(r) \right] f(r) = 0. \tag{16}$$

As discussed in [46], due to the presence of the  $\delta$  function in the Hamiltonian operator in Eq. (11),  $\hat{H}$  is not self-adjoint in general, and singular solutions must be obtained through the self-adjoint extension method [46, 47]. However, it can be shown that the Hamiltonian is essentially self-adjoint if  $|L| \geq 1$ , and thus, we can neglect the influence of the  $\delta$  function and consider only the regular solutions [46, 48] in Eq. (16). In fact, for a quantum ring in the mesoscopic regime, we can assert that  $L > 1$  and, consequently, the eigenfunctions and eigenvalues of the system are given by [32, 49]:

$$\begin{aligned}
\chi_{n,m}(r, \varphi) &= \frac{1}{\lambda} \sqrt{\frac{\Gamma(L+n+1)}{2^{L+1}\pi [\Gamma(L+1)]^2 n!}} \left( \frac{r}{\lambda} \right)^L \\
&\times e^{-\frac{1}{4}\left(\frac{r}{\lambda}\right)^2} {}_1F_1 \left( -n, L+1, \frac{1}{2} \left( \frac{r}{\lambda} \right)^2 \right) e^{im\varphi}, \tag{17}
\end{aligned}$$



(a)  $\alpha = 1$



(b)  $\alpha = 0.7$

FIG. 2: (Color online) Energy eigenvalues of the quantum ring near  $E_F = 0.5$  meV as a function of the magnetic field  $B$  for flat (a) and curvature (b) cases. Each curve denotes a specific  $\chi_{n,m}$  state, and each color represents different subbands. In Figs. 2a and 2b, we plotted the subbands  $n = 0$  (red) and  $n = 1$  (orange). The dashed line locates the Fermi level.

$$E_{n,m} = \left( n + \frac{1}{2} + \frac{L}{2} \right) \hbar\omega - \frac{(m-l)}{2} \hbar\omega_c - \frac{\mu}{4} \omega_0^2 r_0^2, \tag{18}$$

where  ${}_1F_1$  is the confluent hypergeometric function of the first kind,  $n = \{0, 1, 2, 3, \dots\}$  is the radial quantum number which denotes the subband level, and  $m = \{\dots - 2, -1, 0, 1, 2, \dots\}$  is the orbital quantum number which specifies the position in the subband. Note that  $\alpha$  directly modulates the influence of the magnetic field since the flux of  $B$  through the surface enclosed by the ring reduces as  $\alpha$  decreases. For  $\alpha = 1$ , we recover previously reported results [50].

In Figs. 2a and 2b, we plot energy levels of the system as a function of the magnetic field for the cases of  $\alpha = 1$

(flat) and  $\alpha = 0.7$ , respectively. Each curve matches a specific value of both quantum numbers  $n$  and  $m$ , where we are using different colors to represent the levels  $n = 0$  (red) and  $n = 1$  (orange). Note that the border between regions with different colors outlines the behavior of the subband minimum with  $B$ .

As the magnetic field varies at 0K, electrons in the ring perform transitions upon reaching a state crossing point to maintain their most stable configuration. Being  $r_{n,m} = \sqrt{2L}\lambda$  the average radius of a state, these transitions generate an oscillation in their energies, known as Aharonov-Bohm (AB) oscillations, with period  $p_0 = \phi_0/\pi r_{n,m}^2 \approx 2.037\text{mT}$  around  $0.5\text{meV}$  and  $\phi_0 = h/e$  being the quantum of flux [43]. One can identify that, as the

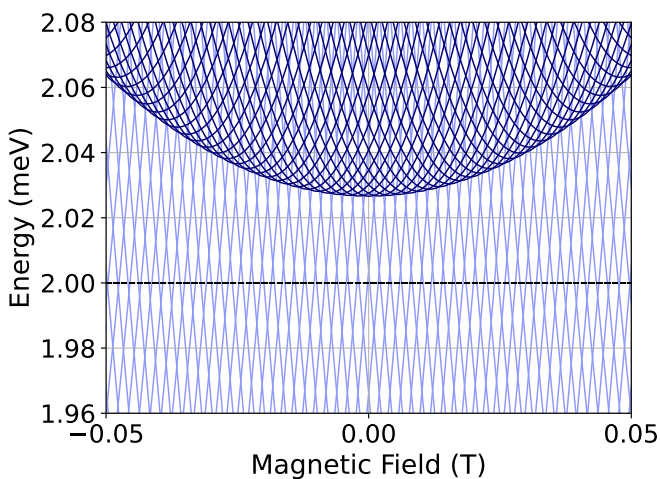
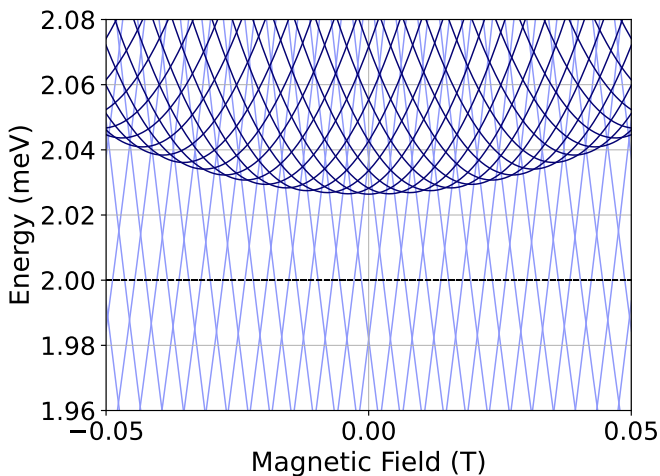
(a)  $\alpha = 1$ (b)  $\alpha = 0.7$ 

FIG. 3: (Color online) Energy eigenvalues of the quantum ring near  $E_F = 2\text{meV}$  as a function of the magnetic field  $B$  for flat (a) and curvature (b) cases. We plotted the subbands  $n = 3$  (light blue) and  $n = 4$  (dark blue). We have omitted the states from the lower subbands ( $n \leq 2$ ) for better visualization.

curvature in the surface increases, the period of the AB oscillations rises by  $p_0/\alpha^2$  [32, 43, 49] as a consequence of its dependence with the area  $\pi(\alpha r_{n,m})^2$  enclosed by the loop. On the other hand, the density of states per unit of energy reduces as a result of the growth in the gap between energetic neighbors already observed in [49].

In Figs 3a and 3b, we perform the same analysis for a regime of four occupied subbands, where states near  $E_F = 2\text{meV}$  from  $n = 3$  (light blue) and  $n = 4$  (dark blue) are highlighted, omitting those from the lower levels to obtain a better visualization of the energy spectrum. A comparison between the flat and curvature cases shows us the same aspects discussed before about the AB period and density of states. However, this situation also provides us with another effect of the modified surface, which can be identified by a reduction in the increment rate of subband minimum  $n = 4$  with the strength of the magnetic field. This is a consequence of attenuation in the influence of  $\mathbf{B}$  from the conical geometry, as expected in Eq. (13). Indeed, we can see no significant change when  $B = 0$ .

As we will explore in the next sections, the three factors mentioned above: AB periods, density of states per unit of energy and subband minimum are going to have important functions in the manifestation of the properties we are investigating.

### III. LANDAUER FORMULA AND RESONANT TUNNELING ON WEAKLY COUPLED RING

Classically, one should expect the conductance  $G$  of a one-dimensional channel to diverge as its length approaches zero. This would not be a surprise since the influence of scattering vanishes as the dimension reduces significantly. However, even for a perfect conducting channel,  $G$  has a finite value,  $G_Q = 2e^2/h$ , known as the *quantum of conductance* [51, 52]. Alternatively, this can be characterized in terms of its reciprocal  $R_Q \approx 12.906\text{k}\Omega$ . If the channel is not a perfect conductor, which can be interpreted as having a single barrier, the probability for an electron with a Fermi energy  $E_F$  to pass through it is  $\mathcal{T}(E_F)$ . The conductance of the channel is then expressed by the *Landauer formula* [53]

$$G(E_F) = (2e^2/h)\mathcal{T}(E_F), \quad (19)$$

where for multiple channels,  $\mathcal{T}(E_F) = \sum_{n,m} \mathcal{T}_{n,m}(E_F)$  with  $n$  and  $m$  denoting the transversal states (17).

In the situation depicted in Fig. 1a, two leads are weakly coupled to the ring. They connect the device to two reservoirs and the contact points with the ring act as a double barrier (two barriers in a series). The system has a non-zero temperature of  $40\text{mK}$  and electrons are subject to loose phase coherence while traveling through the conductor path due, for instance, to scattering of electrons by phonons [51, 54–56], impurities [57], electron-electron interactions [58] and interfacial roughness [59, 60].

Despite that, the decoherence resulting from inelastic scattering in this temperature regime is small enough that we can still expect to observe the effects of phase coherence. Therefore, the Landauer formula should be rewritten as

$$G(E_F) = -(2e^2/h) \sum_{n,m} \int \mathcal{T}_{n,m}(E) \frac{d}{dE} f(E - E_F) dE, \quad (20)$$

where  $f(E - E_F)$  is the Fermi-Dirac distribution and the integral is taken in an arbitrarily small interval centered at  $E_F$  to avoid states that contribute no net current upon application of an electric field through the conductor [52]. When  $T = 0\text{K}$ , we recover Eq. (19). Our aim now is to obtain an expression for  $\mathcal{T}_{n,m}(E)$  which will be, in general, a combination of both coherent and incoherent transmissions,  $\mathcal{T}_c$  and  $\mathcal{T}_d$  respectively.

In a double-barrier configuration, as the width of the well  $W$  becomes smaller, the system acts as a filter, allowing states with a specific energy to pass through the barriers with very high probability even if their transmission coefficients combined are nearly zero. If each barrier has transmission probabilities  $T_1$  and  $T_2$ , reflection probabilities  $R_1 \approx 1$  and  $R_2 \approx 1$ , and if an inelastic scattering factor  $\exp(-2\gamma W)$  has to be included every time the electron traverses the ring path, the coherent transmission coefficient in the regime of  $\gamma \ll W^{-1}$  (low scattering) near the resonant condition is given by [52]

$$\mathcal{T}_c(E) = \frac{\Gamma_1 \Gamma_2}{(E - E_{n,m})^2 + (\Gamma_1 + \Gamma_2 + \Gamma_\phi)^2/4}, \quad (21)$$

where, if the electrons are reflected back and forth between the barriers with a velocity  $v$ ,

$$\frac{\Gamma_1}{\hbar} = T_1 \nu, \quad \frac{\Gamma_2}{\hbar} = T_2 \nu \quad \text{and} \quad \frac{\Gamma_\phi}{\hbar} = (4\gamma W) \nu. \quad (22)$$

In this expression,  $\nu = v/2W$  is the frequency of an electron impinging on one of the barriers and  $2\gamma$  denotes the rate of inelastic scattering per round-trip,  $2W$ . The quantities  $\Gamma_1$  and  $\Gamma_2$  are known as the elastic broadenings, and  $\Gamma_\phi$  is referred as the inelastic broadening. Thus,  $\Gamma_1/\hbar$  and  $\Gamma_2/\hbar$  can be interpreted as the number of times per second an electron successfully passes through the two barriers. Similarly,  $\Gamma_\phi/\hbar$  is the number of times per second the particle is inelastically scattered along the path.

The incoherent component of the transmission, on the other hand, is written as [54]

$$\mathcal{T}_d(E) = \frac{\Gamma_\phi}{(\Gamma_1 + \Gamma_2)} \left\{ \frac{\Gamma_1 \Gamma_2}{(E - E_{n,m})^2 + (\Gamma_1 + \Gamma_2 + \Gamma_\phi)^2/4} \right\}. \quad (23)$$

Thus, we can compute the complete transmission coefficient for each channel,  $\mathcal{T}_{n,m}(E)$ , as

$$\mathcal{T}_{n,m}(E) = \frac{\Gamma_1 \Gamma_2}{(\Gamma_1 + \Gamma_2)} \frac{(\Gamma_1 + \Gamma_2 + \Gamma_\phi)}{[(E - E_{n,m})^2 + (\Gamma_1 + \Gamma_2 + \Gamma_\phi)^2/4]}. \quad (24)$$

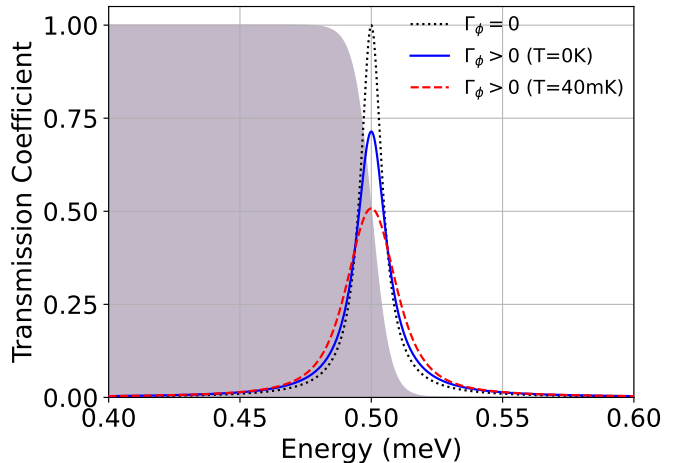


FIG. 4: (Color online) Plot of the expression for the transmission coefficient per energy state given by Eqs. (20) and (24). We have set  $\Gamma_1 = \Gamma_2 = 0.005\text{meV}$  and  $\Gamma_\phi = 0.004\text{meV}$ . The shaded area represents the Fermi-Dirac distribution at 40 mK.

Finally, Eqs. (21) and (23) imply that the correspondent parcels from the coherent and incoherent transmissions related to the total transmission are, respectively,  $(\Gamma_1 + \Gamma_2)/\Gamma$  and  $\Gamma_\phi/\Gamma$  with  $\Gamma = \Gamma_1 + \Gamma_2 + \Gamma_\phi$ .

In Fig. 4, we show the complete transmission coefficients in terms of the energy for both coherent and sequential ( $\Gamma_\phi > 0$ ) tunneling. As expected, we obtain the shape of a Lorentzian with a peak centered at the Fermi level of 0.5 meV. When there is only elastic scattering inside the conductor, electrons near  $E_F$  have  $\approx 100\%$  transmission probability. As we consider inelastic scattering and temperature effects in the system, the peak shifts downward and the Lorentzian broadens, increasing the probabilities for those states further from  $E_F$ . If we set  $\Gamma_1 = \Gamma_2 = 0.005\text{meV}$  and  $\Gamma_\phi = 0.004\text{meV}$  at 40 mK, the transmission peak decays to  $\approx 50\%$ .

In the context of the conical geometry, the elastic broadenings must suffer a correction of  $1/\alpha$  due to the influence of curvature in width  $W$  between the barriers. However, no influence should be observed in the inelastic broadening since it has an increase in attempt frequency.

## IV. RESULTS

To obtain and evaluate the results related to the electric charge transport in the system, we consider the parameter values used in Ref. [43] to mimic the experimental device developed from Ref. [40]. We then set  $\hbar\omega_0 = 0.4496\text{meV}$  and  $r_0 = 800\text{nm}$ . Thus, we have a flat ring width  $\Delta r = 300\text{nm}$  for a Fermi energy of 2 meV and  $\Delta r = 150\text{nm}$  for  $E_F = 0.5\text{meV}$ . In a GaAs sample, the electron effective mass is  $\mu = 0.067m_e$ , where  $m_e$  is the usual electron mass. Furthermore, in

the context of an experimental temperature of 40mK and a weak field ( $\omega_c \ll \omega_0$ ), we set the elastic broadenings to  $\Gamma_1 = \Gamma_2 = (0.005/\alpha)$ meV. We ignore, for simplicity, both dependencies on the magnetic field and quantum numbers for  $\Gamma_1$ ,  $\Gamma_2$  and  $\Gamma_\phi$  [43]. Note that if  $T_1 = T_2 = 0.01$ , the probability of an electron being inelastically scattered through a round trip would be approximately  $4\gamma W=0.008$ , which seems to be a high chance compared to the barriers transmission coefficients combining for 0.0001. However, in the resonant condition (24), we are concerned with states near  $E_F$  which are able to carry net current so that for the significant contributions in the transmission,  $\mathcal{T}_{n,m} > 4\gamma W$ .

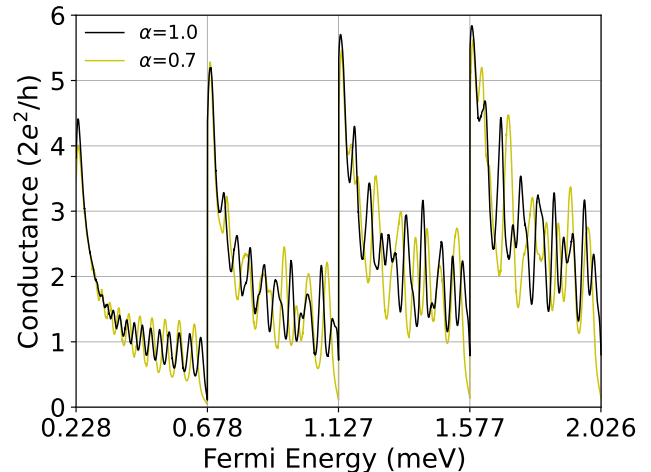
### A. Conductance and Van-Hoove Singularities

Fig. 5a shows the conductance behavior as a function of the Fermi energy for the cases of a curved and a flat ring. This plot is deeply relevant for experimental characterization on the device since  $E_F$  can be set by a gate voltage that controls the number of electrons occupying the system [40, 61, 62]. The peaks result from the high density of states near the bottom of each subband (see Fig. 2) and are known as the Van-Hoove singularities [51]. The total conductance curve then performs an oscillating decay until the Fermi level reaches the bottom of the following subband, generating another peak. Thus, one can directly measure, to high accuracy, the quantity  $\hbar\omega_0$  that characterizes the confinement. The noisy oscillations after the second singularity result from the complex transitions due to the superposition of states from different  $n$  levels.

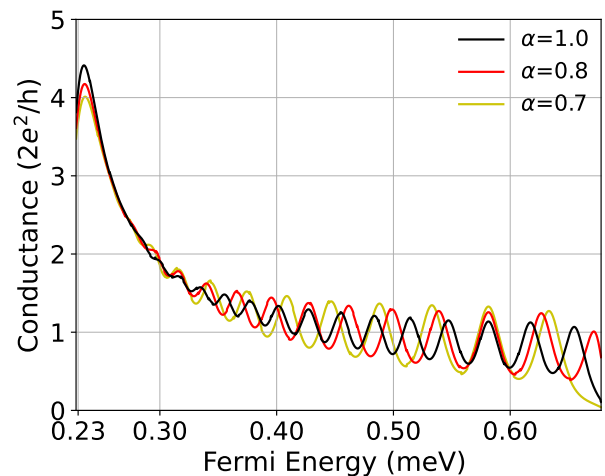
As we have seen in Figs. 2a and 2b, the conical geometry reduces the density of states per unity of energy and increases the gap between state crossing points. Thus, from Eq. (24), both amplitudes and periods of the conductance oscillations should grow with a reduction in  $\alpha$  as is clearly noticeable in Fig. 5b. The Van-Hoove singularities are also affected by a downward shift of their peaks as the curvature parameter decreases. Note that the average value of the conductance always increases from one peak to another due to the cumulative contributions from the lower subbands.

### B. Magnetoresistance

We now turn to analyze the magnetoresistance of the system. In Fig. 6, we plot its behavior with the magnetic field for different values of curvature parameter and two regimes of subband occupation: one (0.5meV) and four (2meV). One can identify an interference pattern distinctive from a beating effect for the lower energy case (red curve). In Figs. 2a and 2b, we can note that the energy of the states can shift upward or downward with  $B$  as a result of the clockwise or anti-clockwise directions of motion of the electrons as they resist the change in the



(a)



(b)

FIG. 5: (Color online) (a) Conductance as a function of the Fermi energy for flat and curvature regime. The peaks result from the density of states per unity of energy [51]. (b) Enlarged plot of Fig. 5a for the first subband.

flux of magnetic field through the internal surface defined by the ring [43, 63].

As discussed previously, near  $E_F$ , the contribution from each state to the magnetoresistance is an AB oscillation with period  $\approx 2.037$  mT. However, their periods acquire a slight difference with the variation in  $n$  and  $B$  [43]. Therefore, since we have only two sets of oscillations for one occupied subband, the sum of all the contributions results in the characteristic beating pattern presented. Since we have four occupied levels for the higher energy case (light blue curve), the superposition of eight sets of oscillations providing state transitions between different subbands will result in apparently noisy oscillations and complex envelope patterns [43].

The effects of curvature in this property are notice-

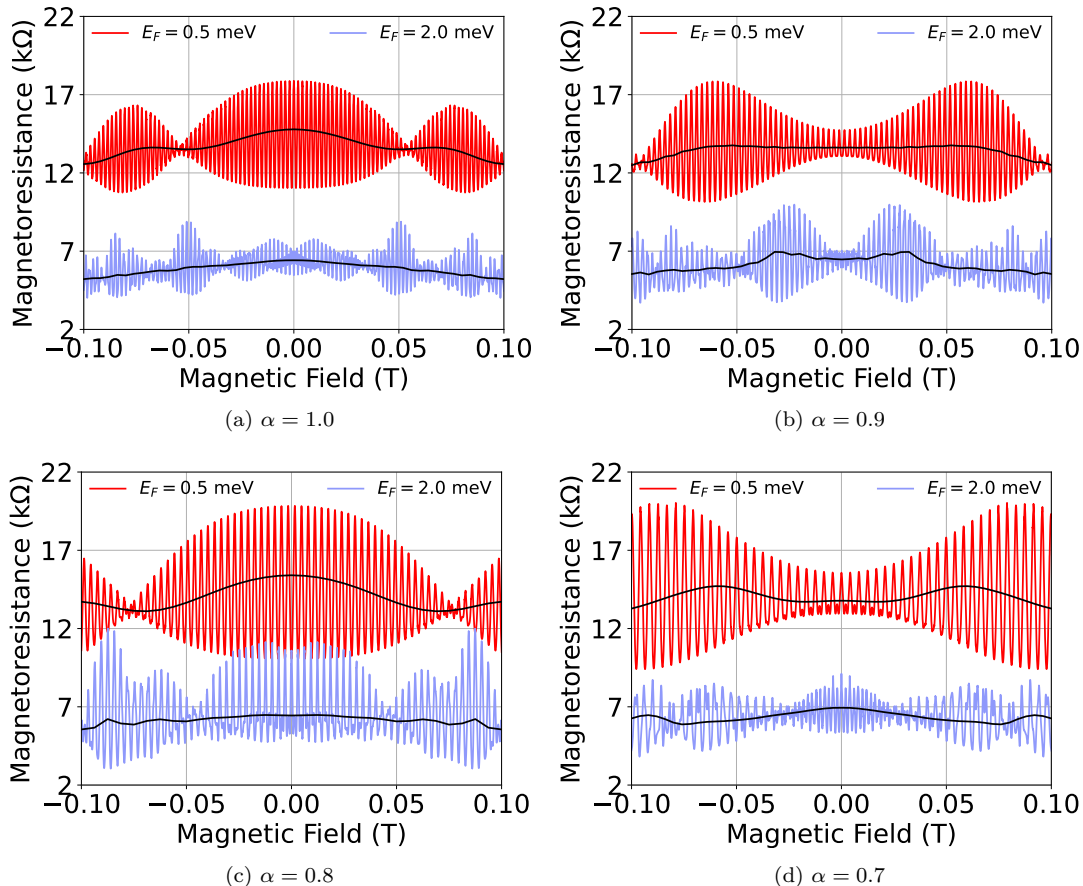


FIG. 6: (Color online) Magnetoresistance as a function of the magnetic field for different values of curvature parameter  $\alpha$ . The average curve points were obtained using intervals of 5 mT.

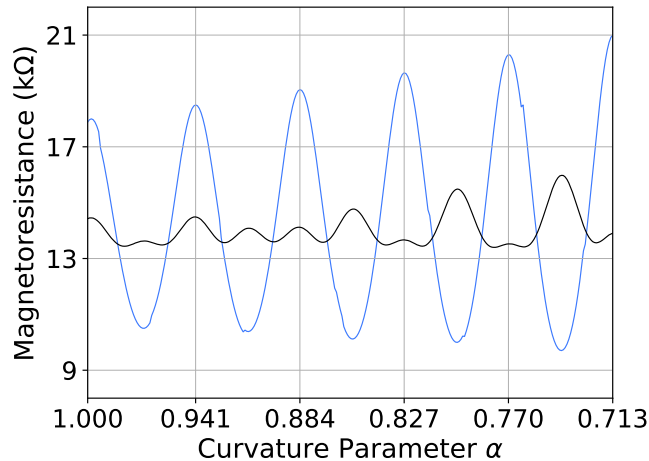
able by following the behavior of the envelope functions. The conical geometry increases the maximum amplitudes of the AB oscillations (antinodes) and their period by  $\approx p_0/\alpha^2$ . These amplitude peaks occur when the Fermi energy matches, in a certain interval of the magnetic field, the curve connecting state crossing points with very similar energies (Fig. 2a). On the other hand, the lowest amplitude regions represented by the nodes occur when  $E_F$  is located in the very middle region between these curves (Fig. 2b) and are dominated by oscillations with period  $p_0/2\alpha^2$  [63].

As we see by comparing Figs. 2a and 6a, the 0.5 meV dashed line nearly passes through the curve defined by the state crossing points when 0 T and, thus, we have an antinode. A similar situation happens to  $\alpha = 0.8$  in Fig. 6c. Conversely, comparing Figs. 2b and 6d for the case of  $\alpha = 0.7$ , Fermi energy is located approximately between these curves, providing an amplitude node, for which a similar pattern can be observed in Fig. 6b. These pattern recurrences can be interpreted as the first indication of a periodic dependence in the magnetoresistance with  $\alpha$ .

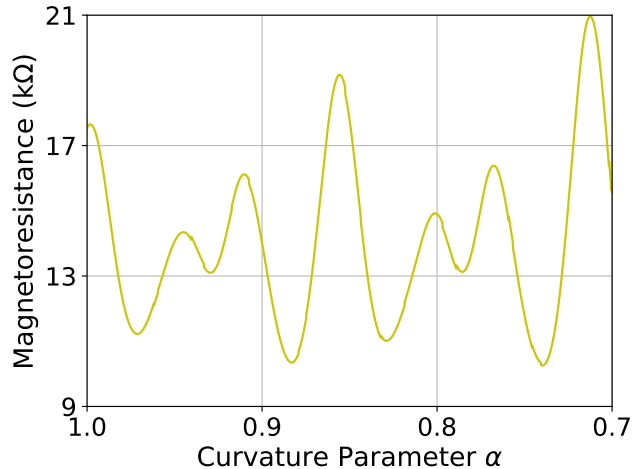
More evidence of this dependence can be found by analyzing the averaged magnetoresistance (solid black curve) in Fig. 6 obtained through intervals of 5 mT, where we

can identify an oscillatory variation of this quantity with  $\alpha$  for several values of  $B$ . Furthermore, it is important to note that the most stable regimes for the averaged magnetoresistance are carried by the nodes, whereas the local peaks in the curve localize the antinodes with good precision.

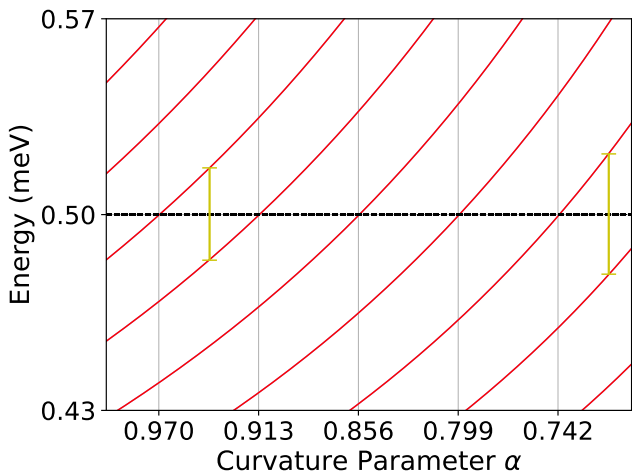
Looking directly at the  $E_F = 2$  meV regime, we highlight that, as Figs. 3a and 3b suggest Fermi energy is near the bottom of the next subband and, even though we are not concerned with the current itself, if one decides to apply a weak and constant electric field along the ring path, the variation in the momentum of an electron,  $\Delta\langle\hat{p}\rangle \approx \Delta m(\hbar/r_{n,m})$  happens only through the variation in angular quantum number [52]. Note that we have not considered the variation in  $r_{n,m}$  since  $L$  has no significant change for small displacements  $\Delta m$  occurring in the same subband. Thus, the electrons can not access a different level through just an applied voltage, and the states from the subband  $n = 5$  are not allowed to be occupied, as well as the  $n \leq 4$  ones with energy above its bottom since they can only be reached by transitions through the states in this forbidden subband. For that reason, we should not take these states into account in Eq. (24) and, therefore, the effect of curvature in the



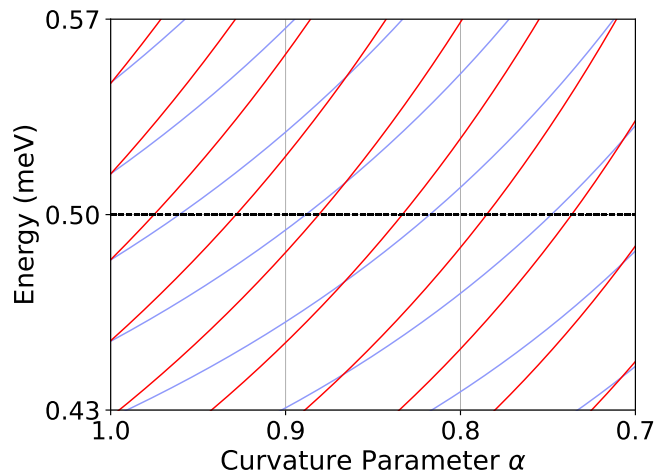
(a)



(a)



(b)



(b)

FIG. 7: (Color online) (a) Magnetoresistance of the system at 0 T (light blue) and its average (dark) as a function of the curvature parameter. The characteristic period of oscillation in  $\alpha$  is approximately 0.057. (b) Energy eigenvalues as a function of the curvature parameter. The crossing points between the energy curves and Fermi level localize the conductance peaks in (a). The yellow vertical bars represent the energy gap between the energetic neighbor states nearest  $E_F$  in the configuration of the local maximum for the resistance.

bottom of this subband plays an important role in the behavior of the magnetoresistance shown in Fig 6.

### C. Magnetoresistance Oscillations in $\alpha$

In Fig. 7a, we present an almost periodic behavior of the magnetoresistance with the curvature for  $B = 0$  (light blue curve). The period of these oscillations  $\Delta\alpha$  is approximately 0.057, which refers to a  $\approx 20.52^\circ$  angular deficit in the material [49]. After a slight increase in

FIG. 8: (Color online) (a) Magnetoresistance as a function of the curvature parameter for  $2p_0 \approx 4.074$  mT. (b) Energy eigenvalues as a function of the curvature parameter for  $2p_0$ . The red curves represent the  $m \geq 0$  states, and the light blue curves the  $m < 0$  states.

the resistance until  $\alpha \approx 0.998$  ( $0.72^\circ$ ), the conductance grows until it achieves its first peak at  $\alpha \approx 0.970$  ( $10.8^\circ$ ). Thus, the charge transport through the ring device can be optimized through specific regimes of deformations in the material structure. Each peak in the oscillating pattern is due to the Fermi energy being energetically in the middle between two state crossing points. On the other hand,  $E_F$  is located exactly in a state crossing point for the valleys, at which we have the configuration where conductance is maximum.

The periodicity can be explained by the intersections of the Fermi level with the energy eigenvalues as we vary  $\alpha$ . This can be visualized in Fig. 7b, where we also can identify an enlarging rate for gaps between energetic neighbor



states around  $E_F$ . This is responsible for increasing the amplitudes of the resistance (i.e., the lift in the peaks). The amplitudes of conductance, however, also increase due to the effect of curvature in the elastic broadenings.

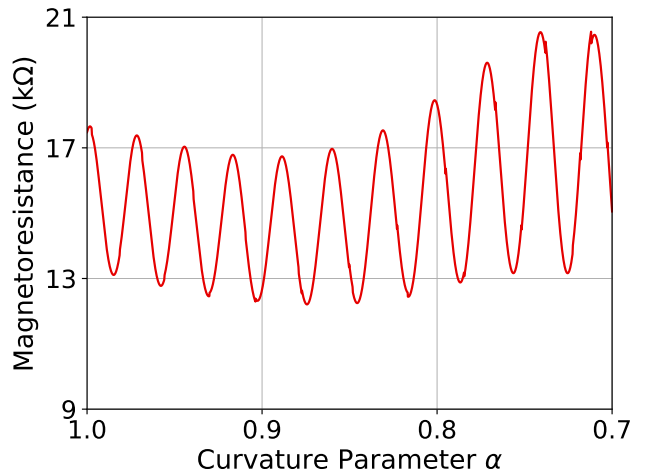
The averaged magnetoresistance (black curve) also provides us with an oscillating pattern for the antinodes (peaks), which, compared with Fig. 6, is in good agreement with our previous assumption that the antinodes carry the local maximums of this quantity. The period of recurrence for antinodes is  $\approx \Delta\alpha/2$ . This periodicity is also valid for the nodes, which cannot be interpreted as the valleys in the same curve. The first node can be achieved for  $\alpha \approx 0.984$  or  $5.76^\circ$  in angular deficit, providing a reduction in the amplitude around  $B = 0$  of 92.6% compared to the flat case. Thus, configurations of stable resistance against external magnetic field fluctuations can be achieved by tuning the curvature parameter.

In the situation where the magnetic field is not zero, Fig. 8b show us that, for  $B = 2p_0$ , the energy eigenvalue curves are split into components of  $m \geq 0$  (red) and  $m < 0$  (light blue). The dynamics of intersection and interference between  $E_F$  and these curves becomes complex, resulting in different patterns of oscillations presented in Fig. 8a, which are not periodic anymore. The increasing amplitudes are explained for the same reasons as the  $B = 0$  case.

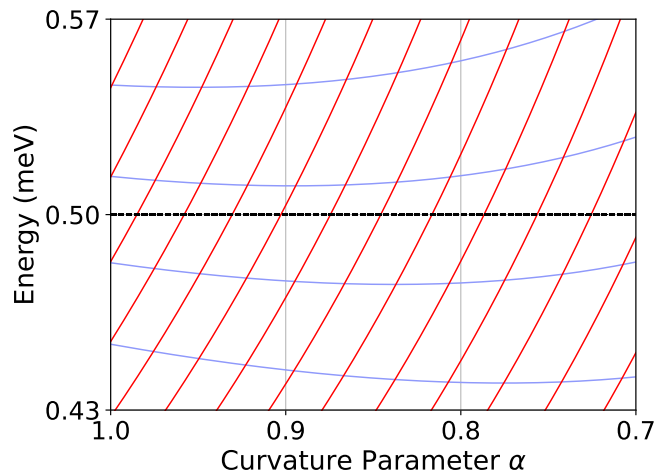
As the value of  $B$  intensifies to  $10p_0$ , the angle between  $m \geq 0$  and  $m < 0$  curves (Fig. 9b) increases in such a way that only the first ones are crossed by the Fermi level until  $\alpha = 0.7$ . Thus, oscillations are mainly governed by these intersections while the characteristic up and down behavior shown in Fig. 9a is determined by both the approximation and the deviation of the  $m < 0$  energies from  $E_F$ . Furthermore, comparing Figs. 7b, 8b and 9b, we can identify that the number of intersections between the 0.5 meV line with the red curves determines the number of conductance peaks. Thus, the higher the value of  $B$ , the higher the number of intersections in a given interval of  $\alpha$ , and, consequently, more oscillations will be observed.

## V. CONCLUSIONS

As we have seen, modifications in the geometry of the device can lead to several implications in the electric charge transport properties. We started by considering the Tan-Inkson model for confining the two-dimensional electron gas. We then let the surface acquire a conical shape where, as immediate consequences, the system had the influence of the background magnetic field attenuated, the eigenenergies suffered a lift coming from the factor  $m^2/\alpha^2$  in  $L$ , and the particles experienced a purely geometrical potential of attractive nature to the ring center. Effects in the energy spectrum were observed as a reduction in the density of states per unity of energy, an increase in the Aharonov-Bohm oscillations period, and a retrenchment in the evolution of the subband bottoms.



(a)



(b)

FIG. 9: (Color online) (a) Magnetoresistance as a function of the curvature parameter for  $B = 10p_0 \approx 20.37$  mT. (b) Energy eigenvalues as a function of the curvature parameter for  $B = 10p_0$ . The red curves represent the  $m \geq 0$  states, and the light blue curves the  $m < 0$  states.

In the resonant tunneling process of the charged particles between the emitter and the collector acting as two barriers, we argued that the inelastic broadening  $\Gamma_\phi$  is not affected by the curvature since the effect in the ring path  $2W$  is canceled as the attempt frequency grows. However, since the elastic broadenings depend only on  $\nu$ , the coherent component of the transmission increases its impact over the incoherent part.

The downward shift observed in the peaks of the conductance Van-Hoove singularities and the increase in both period and amplitude from the oscillating decay with the Fermi level are well described by the effect of curvature in the density of states per unity of energy. No influence from  $\alpha$  was noticed in the distance between

TABLE I: Curvature parameter values for significant configurations of the magnetoresistance oscillations at  $B = 0$ 

	$\alpha_1$	$\alpha_2$	$\alpha_3$	$\alpha_4$	$\alpha_5$	$\Delta\alpha$
Resistance Peaks	0.998	0.941	0.884	0.827	0.770	0.057
Conductance Peaks	0.970	0.913	0.855	0.798	0.741	$0.057 \pm 0.001$
Amplitude Anti-nodes	0.998	0.970	0.941	0.913	0.884	$0.0285 \pm 0.001$
Amplitude Nodes	0.984	0.956	0.927	0.899	0.870	$0.0285 \pm 0.001$

the peaks, preserving the experimental measure of the quantity  $h\omega_0$ .

The beating pattern presented by the magnetoresistance oscillations as a result of the interference from the different sets of motion performed by the electrons revealed to be susceptible to variations in the geometry through an increase in both period and amplitude. The dynamics in the envelope functions can be extremely useful since the average resistance finds its lowest values in the nodes while the highest ones are located in the antinodes. Their recurrence can be controlled by suitable adjustments in the curvature parameter from intervals of  $\Delta\alpha/2$  for  $B = 0$ , presented in TABLE I.

Another remarkable feature observed was the almost periodic oscillation of the magnetoresistance with the curvature parameter, with period  $\Delta\alpha = 0.057$  when there is no external magnetic field. The resistance and conductance peaks are separated by displacements of  $\Delta\alpha/2$  (TABLE I) and have their amplitudes continuously increased as a consequence of the effects in both density of

states and elastic broadenings. For the cases of  $B \neq 0$ , these oscillations are not periodic due to the interference of the  $m < 0$  states and can present distinct patterns depending on the value of  $B$ .

## ACKNOWLEDGMENTS

The authors would like to express gratitude to the Brazilian agencies CAPES, CNPq, FAPEMA, and the NSF agency. Francisco A. G. de Lira acknowledges the support from the grant CAPES/PDSE 44/2022. Edilberto O. Silva acknowledges the support from the grants CNPq/306308/2022-3, FAPEMA/UNIVERSAL-06395/22, FAPEMA/APP-12256/22 and Coordenação de Aperfeiçoamento de Pessoal de Nível Superior - Brazil (CAPES) - Code 001. C.D. Santangelo acknowledges support from the NSF grant DMR 2217543. We are also thankful to Manoel M. Ferreira Jr. for useful comments.

- 
- [1] Y. Aharonov and D. Bohm, Significance of electromagnetic potentials in the quantum theory, *Phys. Rev.* **115**, 485 (1959).
- [2] D. Kahng and M. M. Atalla, Silicon-silicon dioxide field induced surface devices, *IRE-AIEEE Solid-State Device Research Conference, Carnegie Institute of Technology, Pittsburgh, PA* (1960).
- [3] T. Ando, Y. Matsumoto, and Y. Uemura, Theory of hall effect in a two-dimensional electron system, *Journal of the Physical Society of Japan* **39**, 279 (1975).
- [4] K. v. Klitzing, G. Dorda, and M. Pepper, New method for high-accuracy determination of the fine-structure constant based on quantized hall resistance, *Phys. Rev. Lett.* **45**, 494 (1980).
- [5] R. B. Laughlin, Quantized hall conductivity in two dimensions, *Phys. Rev. B* **23**, 5632 (1981).
- [6] M. Büttiker, Y. Imry, and R. Landauer, Josephson behavior in small normal one-dimensional rings, *Physics Letters A* **96**, 365 (1983).
- [7] R. Landauer and M. Büttiker, Resistance of small metallic loops, *Phys. Rev. Lett.* **54**, 2049 (1985).
- [8] L. P. Lévy, G. Dolan, J. Dunsmuir, and H. Bouchiat, Magnetization of mesoscopic copper rings: Evidence for persistent currents, *Phys. Rev. Lett.* **64**, 2074 (1990).
- [9] V. Chandrasekhar, R. A. Webb, M. J. Brady, M. B. Ketchen, W. J. Gallagher, and A. Kleinsasser, Magnetic response of a single, isolated gold loop, *Phys. Rev. Lett.* **67**, 3578 (1991).
- [10] D. Mailly, C. Chapelier, and A. Benoit, Experimental observation of persistent currents in gaas-algaas single loop, *Phys. Rev. Lett.* **70**, 2020 (1993).
- [11] S. Russo, J. B. Oostinga, D. Wehenkel, H. B. Heersche, S. S. Sobhani, L. M. K. Vandersypen, and A. F. Morpurgo, Observation of aharonov-bohm conductance oscillations in a graphene ring, *Phys. Rev. B* **77**, 085413 (2008).
- [12] D. S. L. Abergel, V. M. Apalkov, and T. Chakraborty, Interplay between valley polarization and electron-electron interaction in a graphene ring, *Phys. Rev. B* **78**, 193405 (2008).
- [13] M. Huefner, F. Molitor, A. Jacobsen, A. Pioda, C. Stampfer, K. Ensslin, and T. Ihn, Investigation of the aharonov-bohm effect in a gated graphene ring, *physica status solidi (b)* **246**, 2756 (2009).
- [14] W.-C. Tan and J. C. Inkson, Electron states in a two-dimensional ring - an exactly soluble model, *Semicond. Sci. Technol.* **11**, 1635 (1996).
- [15] J. I. Climente, J. Planelles, M. Barranco, F. Malet, and M. Pi, Electronic structure of few-electron concentric double quantum rings, *Phys. Rev. B* **73**, 235327 (2006).
- [16] W.-C. Tan and J. C. Inkson, Magnetization, persistent currents, and their relation in quantum rings and dots,

- Phys. Rev. B **60**, 5626 (1999).
- [17] L. Lafaurie, Y. Suaza, D. Laroze, W. Gutiérrez, and J. Marín, Thermodynamic properties of an artificial molecule quantum rings: Geometric and external field effects, *Physica B: Condensed Matter* **679**, 415786 (2024).
- [18] D. F. Lima, F. dos S. Azevedo, L. F. C. Pereira, C. Filgueiras, and E. O. Silva, Optical and electronic properties of a two-dimensional quantum ring under rotating effects, *Annals of Physics* **459**, 169547 (2023).
- [19] R. J. Young, E. P. Smakman, A. M. Sanchez, P. Hodgson, P. M. Koenraad, and M. Hayne, Optical observation of single-carrier charging in type-II quantum ring ensembles, *Applied Physics Letters* **100**, 082104 (2012).
- [20] C. O. Edet, F. C. E. Lima, C. A. S. Almeida, N. Ali, and M. Asjad, Quantum information of the aharonov–bohm ring with yukawa interaction in the presence of disclination, *Entropy* **24**, 10.3390/e24081059 (2022).
- [21] G. Huang, W. Guo, P. Bhattacharya, G. Ariyawansa, and A. G. U. Perera, A quantum ring terahertz detector with resonant tunnel barriers, *Applied Physics Letters* **94**, 101115 (2009).
- [22] J. Wu, Z. M. Wang, V. G. Dorogan, S. Li, J. Lee, Y. I. Mazur, E. S. Kim, and G. J. Salamo, Effects of rapid thermal annealing on the optical properties of strain-free quantum ring solar cells, *Nanoscale Res. Lett.* **8**, 5 (2013).
- [23] R. J. Warburton, C. Schafflein, D. Haft, F. Bickel, A. Lorke, K. Karrai, J. M. Garcia, W. Schoenfeld, and P. M. Petroff, Optical emission from a charge-tunable quantum ring, *Nature* **405**, 926 (2000).
- [24] M. Abbarchi, C. A. Mastrandrea, A. Vinattieri, S. Sanguinetti, T. Mano, T. Kuroda, N. Koguchi, K. Sakoda, and M. Gurioli, Photon antibunching in double quantum ring structures, *Phys. Rev. B* **79**, 085308 (2009).
- [25] E. Zipper, M. Kurpas, J. Sadowski, and M. M. Maška, Spin relaxation in semiconductor quantum rings and dots—a comparative study, *Journal of Physics: Condensed Matter* **23**, 115302 (2011).
- [26] S. Bellucci and P. Onorato, Crossover from the ballistic to the resonant tunneling transport for an ideal one-dimensional quantum ring with spin-orbit interaction, *Phys. Rev. B* **78**, 235312 (2008).
- [27] D. V. Bulaev, V. A. Geyler, and V. A. Margulis, Effect of surface curvature on magnetic moment and persistent currents in two-dimensional quantum rings and dots, *Phys. Rev. B* **69**, 195313 (2004).
- [28] S. Mendach, O. Schumacher, H. Welsch, C. Heyn, W. Hansen, and M. Holz, Evenly curved two-dimensional electron systems in rolled-up Hall bars, *Applied Physics Letters* **88**, 212113 (2006).
- [29] A. B. Vorob'ev, K.-J. Friedland, H. Kostial, R. Hey, U. Jahn, E. Wiebicke, J. S. Yukecheva, and V. Y. Prinz, Giant asymmetry of the longitudinal magnetoresistance in high-mobility two-dimensional electron gas on a cylindrical surface, *Phys. Rev. B* **75**, 205309 (2007).
- [30] G. Ferrari and G. Cuoghi, Schrödinger equation for a particle on a curved surface in an electric and magnetic field, *Phys. Rev. Lett.* **100**, 230403 (2008).
- [31] S. Pandey, N. Scopigno, P. Gentile, M. Cuoco, and C. Ortix, Topological quantum pump in serpentine-shaped semiconducting narrow channels, *Phys. Rev. B* **97**, 241103 (2018).
- [32] L. F. C. Pereira, F. M. Andrade, C. Filgueiras, and E. O. Silva, Study of electronic properties, magnetization and persistent currents in a mesoscopic ring by controlled curvature, *Physica E: Low-dimensional Systems and Nanostructures* **132**, 114760 (2021).
- [33] M. C. Ribeiro, M. M. Cunha, C. Filgueiras, and E. O. Silva, Quantum particle motion on the surface of a helicoid in the presence of an harmonic oscillator, *Physics Open* **5**, 100045 (2020).
- [34] R. C. T. da Costa, Quantum mechanics of a constrained particle, *Phys. Rev. A* **23**, 1982 (1981).
- [35] Z.-K. Lin, Q. Wang, Y. Liu, H. Xue, B. Zhang, Y. Chong, and J.-H. Jiang, Topological phenomena at defects in acoustic, photonic and solid-state lattices, *Nat. Rev. Phys.* **5**, 483 (2023).
- [36] M. Gutkin, 12 - elastic and plastic deformation in nanocrystalline metals, in *Nanostructured Metals and Alloys*, Woodhead Publishing Series in Metals and Surface Engineering, edited by S. H. Whang (Woodhead Publishing, 2011) pp. 329–374.
- [37] M. Kleman, Cholesteric liquid crystals: Defects, in *Reference Module in Materials Science and Materials Engineering* (Elsevier, 2016).
- [38] B. Dietz, T. Klaus, M. Miski-Oglu, A. Richter, M. Bischoff, L. von Smekal, and J. Wambach, Fullerene  $c_{60}$  simulated with a superconducting microwave resonator and test of the atiyah-singer index theorem, *Phys. Rev. Lett.* **115**, 026801 (2015).
- [39] B. An, S. Fukuyama, K. Yokogawa, M. Yoshimura, M. Egashira, Y. Korai, and I. Mochida, Single pentagon in a hexagonal carbon lattice revealed by scanning tunneling microscopy, *Applied Physics Letters* **78**, 3696 (2001).
- [40] J. Liu, W. Gao, K. Ismail, K. Lee, J. Hong, and S. Washburn, Correlations between aharonov-bohm effects and one-dimensional subband populations in  $gaas/alxgal-xas$  rings, *Physical review. B, Condensed matter* **48**, 15148 (1993).
- [41] H. Silotia, A. Kumari, A. Vashist, and S. Chakraverty, Linear magnetoresistance and weak antilocalization in a  $lav_3/ktao_3$  heterostructure, *Phys. Rev. B* **109**, 245405 (2024).
- [42] J. Koch, S. Sologub, C. Ghosal, T. Tschirner, A. Chatterjee, K. Pierz, H. W. Schumacher, and C. Tegenkamp, Magnetotransport behavior of epitaxial graphene inhomogeneously doped by  $bi(110)$  islands, *Phys. Rev. B* **109**, 235107 (2024).
- [43] W.-C. Tan and J. C. Inkson, Landau quantization and the aharonov-bohm effect in a two-dimensional ring, *Phys. Rev. B* **53**, 6947 (1996).
- [44] A. Poux, L. R. S. Araújo, C. Filgueiras, and F. Moraes, Landau levels, self-adjoint extensions and hall conductivity on a cone, *The European Physical Journal Plus* **129**, 100 (2014).
- [45] A. M. de M. Carvalho, C. Sátiro, and F. Moraes, Aharonov-bohm-like effect for light propagating in nematics with disclinations, *Europhysics Letters* **80**, 46002 (2007).
- [46] F. M. Andrade, E. O. Silva, and M. Pereira, Physical regularization for the spin-1/2 aharonov-bohm problem in conical space, *Phys. Rev. D* **85**, 041701(R) (2012).
- [47] C. R. Hagen, Aharonov-bohm scattering of particles with spin, *Phys. Rev. Lett.* **64**, 503 (1990).
- [48] S. Alberverio, F. Gesztesy, R. Høegh-Krohn, and H. Holden, *Solvable Models in Quantum Mechanics* (Springer-Verlag, 1988).

- [49] F. A. G. de Lira, L. F. C. Pereira, and E. O. Silva, Study on the effects of anisotropic effective mass on electronic properties, magnetization and persistent current in semiconductor quantum ring with conical geometry, *Physica E: Low-dimensional Systems and Nanostructures* **158**, 115898 (2024).
- [50] W.-C. Tan and J. C. Inkson, Magnetization, persistent currents, and their relation in quantum rings and dots, *Phys. Rev. B* **60**, 5626 (1999).
- [51] C. Kittel, *Introduction to Solid State Physics*, 8th ed. (Wiley, 2004).
- [52] S. Datta, *Electronic Transport in Mesoscopic Systems*, Cambridge Studies in Semiconductor Physics and Microelectronic Engineering (Cambridge University Press, 1995).
- [53] R. Landauer, Spatial variation of currents and fields due to localized scatterers in metallic conduction, *IBM Journal of Research and Development* **1**, 223 (1957).
- [54] M. Büttiker, Quantum coherence and phase randomization in series resistors, in *Resonant Tunneling in Semiconductors: Physics and Applications*, edited by L. L. Chang, E. E. Mendez, and C. Tejedor (Springer US, Boston, MA, 1991) pp. 213–227.
- [55] S. Feng, Quantum transport in the presence of phase-breaking scattering: Generalized landauer formula, *Physica A: Statistical Mechanics and its Applications* **168**, 439 (1990).
- [56] X. Wu and S. E. Ulloa, Electron-phonon interaction in double-barrier resonant tunneling, *Phys. Rev. B* **44**, 13148 (1991).
- [57] R. Sirko and D. L. Mills, Free-carrier absorption in *n*-type semiconductors: The inelastic scattering of electrons from ionized impurities, *Phys. Rev. B* **18**, 5637 (1978).
- [58] V. Srivastava and R. Krishnan, Intrinsic phase-decoherence of electrons by two-level systems, *Modern Physics Letters B* **16**, 511 (2002).
- [59] B. Vinter and F. Chevoir, Scattering processes, coherent and incoherent transport in resonant tunneling structures, in *Resonant Tunneling in Semiconductors: Physics and Applications*, edited by L. L. Chang, E. E. Mendez, and C. Tejedor (Springer US, Boston, MA, 1991) pp. 201–211.
- [60] H. Sakaki, T. Noda, K. Hirakawa, M. Tanaka, and T. Matsusue, Interface roughness scattering in GaAs/AlAs quantum wells, *Applied Physics Letters* **51**, 1934 (1987).
- [61] H. van Houten and C. Beenakker, Quantum Point Contacts, *Physics Today* **49**, 22 (1996).
- [62] B. J. van Wees, H. van Houten, C. W. J. Beenakker, J. G. Williamson, L. P. Kouwenhoven, D. van der Marel, and C. T. Foxon, Quantized conductance of point contacts in a two-dimensional electron gas, *Phys. Rev. Lett.* **60**, 848 (1988).
- [63] S. Jo, G. L. Khym, D.-I. Chang, Y. Chung, H.-J. Lee, K. Kang, D. Mahalu, and V. Umansky, Beating of aharonov-bohm oscillations in a closed-loop interferometer, *Phys. Rev. B* **76**, 035110 (2007).